Journal of Materials Science Research and Reviews

8(4): 172-179, 2021; Article no.JMSRR.77207

Synthesization of Monoclinic ($Ba_2MgSi_2O_7$: Dy^{3+}) Structure by Combustion Route

Sanjay Kumar Dubey[1], Shashank Sharma[1*], A. K. Diwakar[1] and Sanjay Pandey[2]

[1]Department of Physics, Kalinga University, Naya Raipur, C.G, India.
[2]Department of Physics, Bhilai Institute of Technology, Raipur, C.G, India.

Authors' contributions

This work was carried out in collaboration among all authors. Authors SKD and SS have their own great contribution and lead role in making this research paper, which includes paper design, research study, data analysis, data collection, sample preparation and its characterization as well as literature survey. All authors SKD, SS, SP and AKD read and approved the final manuscript.

Article Information

Editor(s):
(1) Prof. Yong X. Gan, California State Polytechnic University, USA.
Reviewers:
(1) Manar Ghyath Abd Almutalib Almosawy, Imam Jafaar Al-Sadiq University, Iraq.
(2) Shyan-Lung Chung, National Cheng Kung University, Taiwan.
Complete Peer review History: https://www.sdiarticle4.com/review-history/77207

Original Research Article

Received 08 September 2021
Accepted 18 November 2021
Published 19 November 2021

ABSTRACT

$Ba_2MgSi_2O_7$:Dy^{3+} (BMSD) white light emitting phosphor was sintered by combustion synthesis route. The phase formation was confirmed with the help of XRD characterization. The results of the XRD study obtained for this phosphor revealed its monoclinic crystal symmetry with a space group C2/c. The XRD pattern well matched with the help of JCPDS Pdf file No. 23-0842. The average crystallite size was calculated as 31.63nm and strain as 0.27. Functional group investigation with the help of FTIR spectroscopy and Photoluminescence properties were also discussed. The sintered $Ba_2MgSi_2O_7$:Dy^{3+} (BMSD) phosphor was stimulated at 383nm and their corresponding emission spectra were peaked at blue (477 nm), yellow (574 nm) and red (677nm), three spectral lines because of the $^4F_{9/2}\rightarrow{}^6H_{15/2}$, $^4F_{9/2}\rightarrow{}^6H_{13/2}$, $^4F_{9/2}\rightarrow{}^6H_{11/2}$, transitions of trivalent dysprosium [Dy^{3+}] ions. In this paper, the XRD, FTIR and photoluminescence properties of this phosphor are also investigated in detail.

Keywords: $Ba_2MgSi_2O_7$:Dy^{3+} (BMSD); X-ray diffraction (XRD); Photoluminescence (PL).

**Corresponding author: Email: dr.shashankeinstein@rediffmail.com;*

ABBREVIATION

WLEDs : White Light Emitting diodes
RE : Rare Earths
FTIR : Fourier Transform Infra-Red Spectroscopy
XRD : X-Ray Diffraction
KBr : Potassium Bromide
LEPs : Light emitting phosphors
$Ba_2MgSi_2O_7:Dy^{3+}$: BMSD

1. INTRODUCTION

The combustion synthesis technique is a facile, fast, versatile, cheaper and efficient pathway for rapid production of a broad range of oxides, ceramics, catalysts and nano-sized phosphor materials from a technology point of view [1-3]. As a commercial phosphor, $BaMgAl_{10}O_{17}$: $Eu^{2+}$is prepared by this technique [4]. T. T. H. Tam et al. synthesized divalent europium doped di barium magnesium di silicate phosphor with the help of the Combustion method [5]. Rare-earth doped silicate materials possess high luminescence efficiency [6]. Dysprosium (Dy^{3+}) rare-earth ion plays a prominent role in generating various types of LEPs [7]. For the preparation of WLED phosphors, the combustion technique is used as it confers control over the morphology and particle size of the prepared phosphors [8]. M. Shimizu et al. reported that the pure di barium magnesium di silicate [$Ba_2MgSi_2O_7$] has a tetragonal crystal structure through single-crystal X-ray investigation [9]. $Ba_2MgSi_2O_7$: Ce^{3+}, Tb^{3+} phosphor was synthesized using a one-step solid-state reaction method. The XRD results revealed that the prepared phosphors have a monoclinic crystal structure, and the crystallite size increases with the incorporation of dopants ions [10]. In this experiment, the host phosphor demonstrates a monoclinic crystal structure with the space group C2/c (No. 15) [11]. Among the phosphor discovered so far, the optimum afterglow material is [$SrAl_2O_4$: Eu^{2+}, Dy^{3+}], which is also used as a commercial phosphor. This phosphor may exhibit afterglow for more than 20 hours [12-13]. In silicate phosphors, trivalent dysprosium [Dy^{3+}] can work as both luminescence centre and trap [14, 15]. For the human eye, the divalent europium [Eu^{2+}] doped di barium magnesium di silicate is ideal, making it highly appropriate for practical applications [16, 17]. $Ba_2MgSi_2O_7$, monoclinic crystal structure consists of two-dimensional SiO_4 and MgO_4 tetrahedral layers, which are connected through common corners. Divalent barium [Ba^{2+}] ions are situated between the layers and coordinated by eight oxygen ions [18]. W.B. Dai, Ph.D (2020) et al., reported that the green emission of $BaMgSiO_4$:Eu (BMSO:Eu) phosphor can have numerous potential applications, such as in white light-emitting diodes (WLEDs), bio-imaging and light photo-chromism as well as long-persisting phosphors [19]. Mellite is a large group of compounds characterised through the general structure formula $M_2T^1T^2{}_2O_7$, [where M= Barium (Ba), Strontium (Sr), Calcium (Ca); T^1= Magnesium (Mg), Zinc (Zn), Copper (Cu), Manganese (Mn), Cobalt (Co); T^2 = Germanium (Ge), Silicon (Si)], and has been significantly studied thanks to its impressive stability and structure. Alkaline earth metals such as calcium, strontium and barium rare-earth-doped silicates develop as luminescence phosphors continuously over a longtime, also known as long persistent luminescence phosphors (LPL), which are being studied extensively [20].

In the current analysis, we have successfully synthesized $Ba_2MgSi_2O_7:Dy^{3+}$ (3mol %) phosphor by the simple combustion method exclusively. No other combustion method has been used. The structural and optical properties such as XRD, FTIR and Photoluminescence (PL) spectra for the phosphor are also discussed.

2. EXPERIMENTAL DETAILS

2.1 Sample Preparation

We have used combustion synthesis process in our experiment for the preparation of $Ba_{2-x}MgSi_2O_7$: Dy_x^{3+} (3mol %) (BMSD) phosphor. With (99.99%) purity, Ba $(NO_3)_2$ (Analytical Reagent), Mg $(NO_3)_2$ (Analytical Reagent), SiO_2*H_2O (Analytical Reagent), and rare earth nitrate Dy $(NO3)_3$ (Analytical Reagent) were utilized as starting raw reagents, while urea (NH_2CONH_2) was used as a combustion fuel and H_3BO_3 (boric acid) was also used as a flux. In our experiment, it was essential that all raw chemicals with appropriate molar ratio were dissolved in a very little amount of acetone (CH_3COCH_3) to get a clear solution. Each nitrates, flux and fuel was mixed into agate mortar and pestle (diameter-5'') in clockwise direction (we can mix it in any direction but the choosen direction should be maintained throughout the mixing) for 5 min to convert into a thick paste before being transferred to a silica crucible. Then the mixture was subsequently heated in already maintained muffle furnace at

650^{o}C. The entire combustion synthesis process got completed in approximately 5 min. After a few minutes, the mixture solution undergoes thermal dehydration with release of gaseous products, to form silicates and ignites to produce a self-propagating flame (Fig 1). After next few seconds post its completion, the crucible is taken out of furnace and kept in open for it to be cooled. After cooling, we obtain fluffy form of phosphor, which is then grinded with the help of agate mortar pestle (diameter-5") to obtain material in the powder form. The final product obtained was post-annealed at 1000°C for 1 hour under an air atmosphere. With the help of additional crushing to get fine powder. The resulting specimen was then kept back in airtight bottle for characterization examinations.

The chemical reaction of this entire process as follows:

$$Ba(NO_3)_2 + Mg(NO_3)_2 + SiO_2{*}H_2O + NH_2CONH_2 + Dy(NO_3)_3 \rightarrow Ba_2MgSi_2O_7: Dy^{3+} + H_2O(\uparrow) + CO_2(\uparrow) + N_2(\uparrow) \quad (1)$$

For the combustion process of oxides, metal nitrates were applied as oxidizer and urea is applied as reducer [20]. Thus, the heat of combustion is maximum for Oxidizer/Fuel ratio is equal to 1 [21].

2.2 Sample Characterization

The phase composition of the synthesized phosphor was noted with the help of Bruker D8 advance X-ray diffractometer with Cu-K_α radiation having wavelength (λ = 1.5406, 40 kV, and 40 mA), respectively. Actual formation of this phosphor was obtained through FTIR. An FTIR spectrum was recorded in the range between (4000-400cm^{-1}) with the help of Bruker Alpha Fourier transform infra-red spectroscopy through mixing the sample with analytical reagent potassium bromide (KBr) with pallet preparation. In photoluminescence spectra (PL), emission spectra were recorded by a spectro-fluorophotometer (SHIMADZU, RF-5301 PC) using a xenon lamp of power 150 watt as excitation source. All experiments were performed in identical conditions and the data was collected at room temperature. All required instructions were clearly followed.

3. RESULTS AND DISCUSSION

3.1 X-ray Diffraction (XRD)

XRD patterns were recorded in the range between (10^0\2θ\$80^0$) of $Ba_2MgSi_2O_7$:Dy^{3+} phosphor and synthesized by combustion route. Fig. 2 displays the XRD pattern of BMSD phosphor. All the displayed peaks matched with standard JCPDS PDF file No. 23-0842 [22]. The cell volume the following lattice parameters were also examined [11]. All parameters have shown in Table 1. It is generally agreed through investigations that the influence of doping doesn't affect the phase structure of the phosphors. We have suggested that the trivalent dysprosium [Dy^{3+}] ion as requisite to capture the di valent barium [Ba^{2+}] ion sites in the di barium magnesium di silicate [$Ba_2MgSi_2O_7$] host.

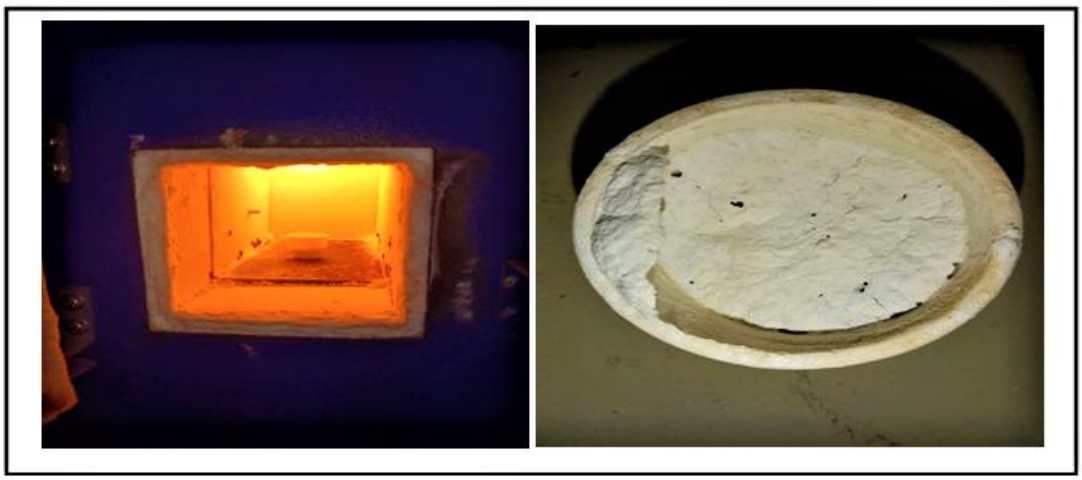

Fig. 1. $Ba_2MgSi_2O_7$: Dy^{3+} Phosphor

Atul D. Sontakke (2020) et al., reported that the crystal structure is composed of discrete $[Si_2O_7]^{6-}$ units which are connected by tetrahedrally coordinated magnesium [Mg] ions, forming two-dimensional sheets in the ac plane and are separated through layers of octahedrally coordinated Barium [Ba] ions. The radial distribution plot reveals the distance and number of available sites of tetrahedrally coordinated Mg^{2+} ions around the octahedrally coordinated Ba^{2+} ions in the monoclinic lattice of $Ba_2MgSi_2O_7$ phosphor [23].

3.1.1 Debye-Scherrer formula

The calculation of average crystallite size (D), with the help of Debye–Scherrer formula, for prominent peak (022) of the BMSD phosphor as shown in Table 1.

Debye–Scherrer formula is represented as follows:

$$D= K\lambda/\beta Cos\theta \quad (2)$$

Where K = 0.94 (Scherrer constant), λ is the wavelength of occurrence X-ray (for Cu Kα, λ = 1.5406 Å), β is the FWHM (Full width half maximum) of the peaks and θ (theta) is represented as the corresponding Braggs diffraction angle [24].

3.1.2 Strain determination by Uniform Deformation Model (UDM)

The strain induced broadening in the powder sample was calculated by the following mathematical relation:

$$\varepsilon = \beta/4tan\theta. \quad (3)$$

3.2 Fourier Transform Infra-Red Spectroscopy

FTIR Spectra

FTIR is a non involving damage, facile and molecular-spectroscopic technical system used for collecting the IR [infra-red] absorption spectrum of the phosphor [25]. The FTIR spectrum of this pure BMS sample has been shown in Fig: 3a and was recorded in the range of (4000 cm^{-1} to 400 cm^{-1}). The band centered at 483.82 cm^{-1}, 564.19 cm^{-1}, 617.23 cm^{-1}, 676.35 cm^{-1}, 837.63 cm^{-1}, 923.36 cm^{-1} and 1026.23 $cm^{-1}$and can be attributed to the presence of silicate $[SiO_4]$ functional group. In addition, considering the absorption bands, validated at 676.35 cm^{-1} and 564.19 cm^{-1}, respectively, because of the presence of $[SiO_4]$ functional group. Thus on examination, we observe that the absorption bands of silicate $[SiO_4]$ functional groups were clearly evident in the (IR) infra-red spectrum. The sharp band centered at 837.63, 923.36 cm^{-1} and 1026.23cm^{-1}can be attributed to the asymmetric strech of Si-O-Si.

The bands allocated at 676.35 cm^{-1} and 617.23 cm^{-1} may be responsible due to the [Si-O] symmetric stretching and [Ba-O] bending vibrations. The bands bending revealed at 564.19 cm^{-1} and 483.82 cm^{-1}, because of the existence of [Si-O-Si] vibrational mode. The Peak centered at 837.63 cm^{-1} may be responsible to [Mg-O] bending vibrations and due to the asymmetric stretching on its spectrum dominates, band allocated at 1656.35 cm^{-1}. The bands centered at 1829.52 cm^{-1}, 1893.86 cm^{-1} and 1968.33 cm^{-1} is responsible for the carbonation reaction mechanism. This can be lead to distortion in the lattice resulting in 1429.49 cm^{-1} and 1656.35 cm^{-1} vibration modes represented to vibration in divalent barium ion $[Ba^{2+}]$ and divalent magnesium ion $[Mg^{2+}]$ respectively. At 3427.61 cm^{-1}, peak centered due to [O-H] hydroxyl group stretching which reveals the presence of moisture in this specimen [26-32].

3.3 Photoluminescence Spectra

The optical Properties including excitation and emission spectra of $Ba_2MgSi_2O_7:Dy^{3+}$ phosphor have displayed in Fig. 3(b) and 3(c) respectively. Trivalent Dy^{3+} ions which displays spectral lines in the (450 to 500nm) blue region because of ($^4F_{9/2}\rightarrow{}^6H_{15/2}$) transition and in the 550 to 600nm yellow region because of the ($^4F_{9/2}\rightarrow{}^6H_{13/2}$) as well as in the (650 to 700nm) red region ($^4F_{9/2}\rightarrow{}^6H_{11/2}$) transition, have attracted much attention, due to the great indication for white light emission in the visible region of electromagnetic spectrum. For the Dy^{3+} single doped $Ba_2MgSi_2O_7$ phosphor, the excitation spectra for the emission at 576nm comprise a series of spectral line in the 300 to 480nm region with the strongest line at 383nm and some other spectral lines at 335nm, 352nm, which are responsible to the transitions from the low energy state to high energy states in the $4f^9$ configuration of Dy^{3+} ions. We observed that these are not clearly allocated because of the dense and overlapping levels of 4f configurations of Dy^{3+} ions in the high energy region [33].

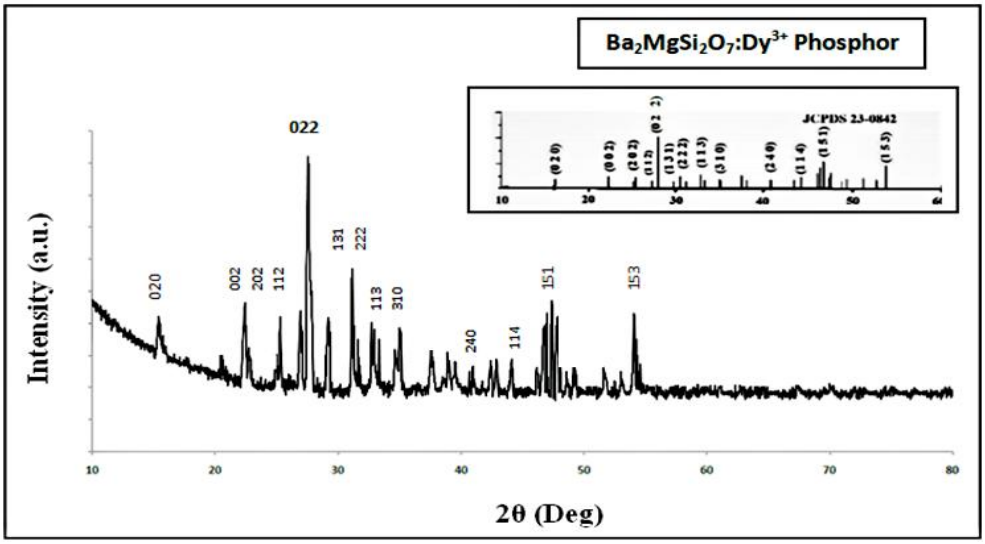

Fig. 2. XRD pattern of $Ba_2MgSi_2O_7:Dy^{3+}$ phosphor.

Table 1. For the highest peak (022), the calculated parameters are shown in below table

No.	Parameters		$Ba_2MgSi_2O_7:Dy^{3+}$
1.	Crystal Structure		Monoclinic
2	Space Group		C2/c
3.	Lattice Parameters	a=8.4128 Å, b=10.7101Å, c= 8.4387 Å,	β=110.71°
4.	Crystallite Size D(nm)		31.63nm
5.	2ɵ[Deg]		27.49
6.	Cell Volume		711 $(Å)^3$
7.	Crystal Plane Spacing d (Å)		3.24268 (Å)
8.	Strain		0.27

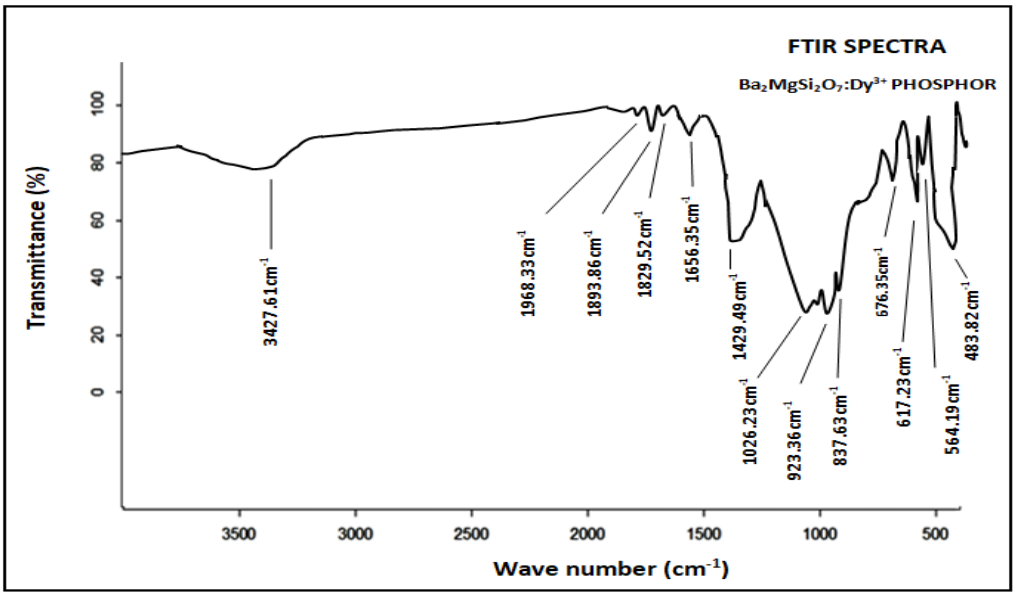

Fig. 3(a). FTIR Spectra of BMSD Phosphor

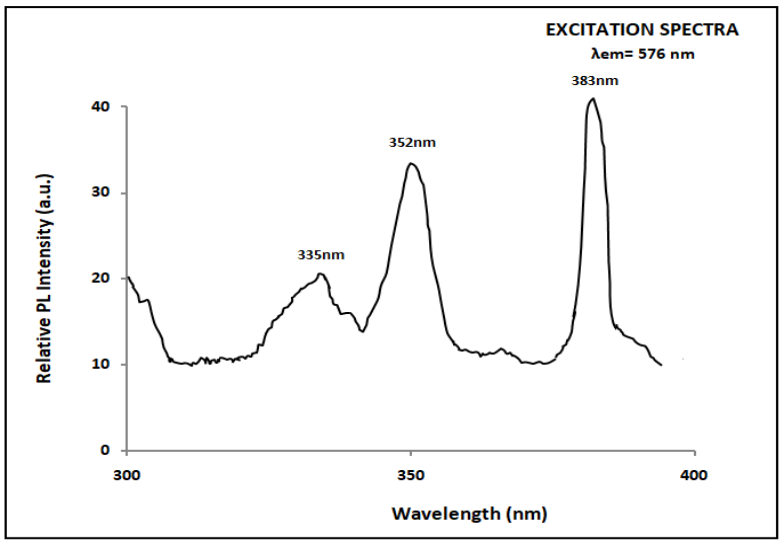

Fig. 3(b). Excitation Spectra of BMSD phosphor

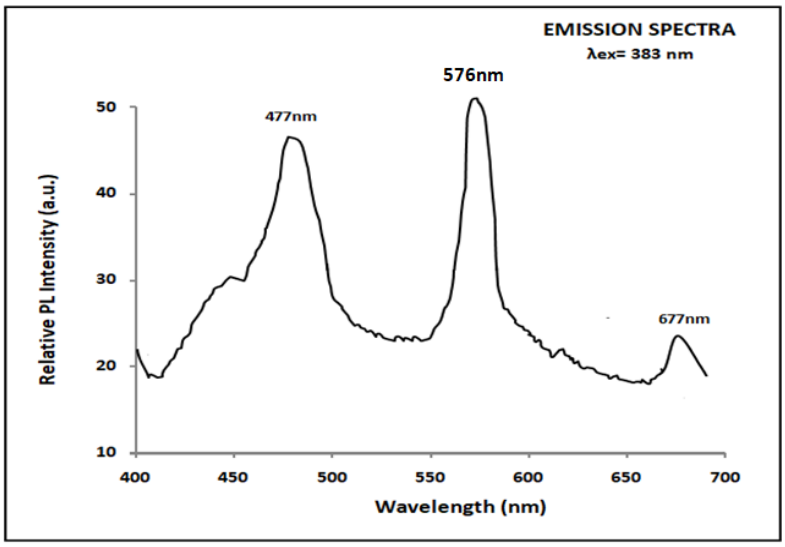

Fig. 3(c). Emission spectra of BMSD phosphor

3.4 Electron or Hole Trap Mechanism

Alkaline earth ion vacancy is considered to be the hole trap, while trivalent Dy^{3+} ion occupying alkaline earth such as (Ca, Ba, Sr) ion sites is a very probable source of electron trap. In our experimental study, after the irradiation with the UV light, most of the stimulation energy associated with the excited charge carriers such as electrons or holes will be transferred through the host (BMS) directly to the luminescence centers. However, part of the stimulation energy will be stored when some of the excited charge carriers drop into the traps, instead to the ground state [33].

The BMSD phosphor exhibited that the higher relative PL emission intensity peaks situated at blue (477 nm) $^4F_{9/2}\rightarrow{}^6H_{15/2}$, yellow (576 nm) $^4F_{9/2}\rightarrow{}^6H_{13/2}$ and red (677nm) $^4F_{9/2}\rightarrow{}^6H_{11/2}$ due to electronic transition respectively. The yellow band emission ($^4F_{9/2}\rightarrow{}^6H_{13/2}$) connected to the forced electric-dipole transition type is permitted only at low symmetry. Synchronously, its intensity is strongly affected by the crystal-field surrounding. The blue band emission ($^4F_{9/2}\rightarrow{}^6H_{15/2}$) is acquired because of the magnetic dipole transition at 477nm wavelength and the red band emission ($^4F_{9/2}\rightarrow{}^6H_{11/2}$) also acquired at 677nm wavelength in emission spectrum corresponds to the dysprosium [Dy^{3+}]

ion [34-37]. The optimum intensity is obtained with 3 mol % doping concentration of dysprosium [Dy^{3+}] ion.

4. CONCLUSION

In summary, $Ba_2MgSi_2O_7:Dy^{3+}$ phosphor was successfully prepared via combustion route and shows greenish-yellow emission. The XRD spectra of the phosphor were well matched with JCPDS file 23-0842. The synthesized phosphor was obtained in nano range with much better homogeneity. Actual formation and the functional group identification of the BMSD phosphor were collected via FTIR spectroscopy. The BMSD phosphor exhibited that the higher relative PL emission intensity peaks at blue (477 nm) $^4F_{9/2}\rightarrow{}^6H_{15/2}$, yellow (576 nm) $^4F_{9/2}\rightarrow{}^6H_{13/2}$ and red (677nm) $^4F_{9/2}\rightarrow{}^6H_{11/2}$ due to electronic transition. These results indicate that synthesized phosphor may be better promising candidate phosphor in the field of solid-state lighting and white light long afterglow applications as well as plasma display panel and Image Processing.

ACKNOWLEDGEMENTS

We gratefully acknowledge the kind support for the facility of XRD analysis Dept. of Metallurgical Engineering and FTIR analysis Dept. of physics, NIT Raipur (C.G.). Authors are also thankful to Dept of physics, Pt. Ravishankar Shukla University, Raipur (C.G.) for providing us the facility of Photoluminescence analysis. We are also heartily grateful to Dept. of physics, Dr. Radha Bai, Govt. Navin Girls College Mathpara Raipur (C.G.), providing the facility of muffle furnace and other essential research instruments.

COMPETING INTERESTS

Authors have declared that no competing interests exist.

REFERENCES

1. Aruna ST, Mukasyan AS. Curr. Opin. Solid State Mater. Sci. 2008;12:44–50. DOI: 10.1016/j.cossms.2008.12.002
2. Patil KC, Aruna ST, Mimani T. Curr. Opin. Solid State Mater. Sci. 2002;6:507–512. DOI: 10.1016/S1359-0286(02)00123-7
3. Patil KC, Hegde MS, Rattan T, Aruna ST. (Eds.); Chemistry of Nanocrystalline Oxide Materials: Combustion Synthesis, Properties and Applicatons; World Scientific: New Jersey, 2008. ISBN: 13 978-981-279-314-0
4. Rogachev AS, Mukasyan AS. (Eds.); Combustion for Material Synthesis; CRC Press: United State. 2014. ISBN: 9781482239515 - CAT# K23274
5. Tam TTH, Du NV, Kien NDT, Thang CX, Cuong ND, Chien ND, Nguyen DH, Huy PT. J. Lumin. 2014;147:358–362.
6. Fernandez-Carrion AJ, Ocana M, Florian P, Garcia-Sevillano J, Cantelar E, Fitch AN, Suchomel MR, Becerro AIJ. Phys. Chem. C, 2013;117(40): 20876-20886
7. Vinicius Ribas De Morais, Preparation Of Dy^{3+} Doped Calcium Magnesium Silicate Phosphors by a New Synthesis Method and Its Luminescence Characterization. In the Proceedings of the 2018, 7th International Congress On Ceramics & 62th Congress Brasileiro De Ceramica, Foz Do Iguacu- Pr Brazil; 2018.
8. Bhatkar VB, Bhatkar NV. Combustion synthesis and photoluminescence study of silicate biomaterials. Bulletin of Materials Science. 2011;34(6):1281-1284.
9. Shimizu M, Kimata M, Iida I. “Crystal structure of $Ba_2MgSi_2O_7$ melilite: The longest tetrahedral Mg-O distance,” N. Jb. Miner. Mh., Jg. 1995;H.1,39.
10. Kanchan Mondal J, Manam. Colour-tunable luminescence and thermal stability of blue-green emitting $Ba_2MgSi_2O_7$: Ce^{3+}, Tb^{3+} phosphors. Journal of Molecular structure. 2020;1215:128262.
11. Aitasalo T, Hölsä J, Laamanen T, Lastusaari M, Lehto L, Niittykoski J, Pellé FZ. Kristallogr. Suppl. 2006;23:481-486.
12. Garlick GFJ, Gibson AF. The electron trap mechanism of luminescence in sulphide and silicate phosphors. Proc. Phys. Soc. Sect. A. 1948;60:574-590.
13. Koen Van den Eeckhout, Philippe F. Smet and Dirk, Poelman. Materials. 2010; 3:2536-2566
14. Chaoshu Shi, Yibing Fu, Bo Liu, G. Zhang, Yonghu chen, Zeming Qi, Xixian Luo, J. Lumin. 2007;122:11.
15. Bo Liu, Linjie Kong, Chaoshu Shi, J. Luminescence. 2007;122:121.
16. Aitasalo T, Hreniak D, Holsa J, Laamanen T, Lastusaari M, Nittykoski J, Pelle F, Strek W. Persistent luminescence of $Ba_2MgSi_2O_7:Eu^{2+}$. J. Lumin. 2007;122–123:110–112.

17. Ravi Shrivastava, Jagjeet Kaur, Vikas Dubey , Beena Jaykumar & Stefano Loreti. Photoluminescence and Thermoluminescence Investigation of Europium- and Dysprosium- Doped Di Barium Magnesium Silicate Phosphor, Spectroscopy Letters: An International Journal for Rapid Communication; 2014. DOI: 10.1080/00387010.2013.872666.
18. Qing–Yang Wang P, Yuan Ting–Wei. Wang, Zhi–Qian. Yin, Fa– Chun. Lu, Effect of Sr, Ca substitution of Ba on the photoluminescence properties of the Eu2+ activated $Ba_2MgSi_2O_7$ phosphor, Ceramics International; 2019. DOI:https://doi.org/10.1016/j.ceramint. 2019.09.100.
19. Dai WB, et al. Journal of Luminescence. 2020;222:117317.
20. Ekamabaram S, Maaza M. J. Alloy. Compd. 395;132; 2005.
21. Kingsley JJ, Patil KC. A novel combustion process for the synthesis of fine particle α-alumina and related oxide materials. Materials letters. 1988;6(11-12):427-32.
22. JCPDS Pdf file number 23-0842, JCPDS International Center for Diffraction Data.
23. Atul D. Sontakke et al. J. Phys. Chem. C 2020;124:13902−13911.
24. Ubale AU, Sangawar VS, Kulkarni DK. Size dependent optical characteristics of chemically deposited nanostructured ZnS thin films. Bulletin of Materials Science. 2007;30(2):147-51.
25. Devender Singh, Suman Sheoran and Vijeta Tanwar. Europium doped silicate phosphors: Synthetic and characterization techniques. Advanced Material Letters. 2007;8(5):656-672.
26. Shannon RD. Revised effective ionic radii and systematic studies of interatomic distances in halides and chalcogenides. Acta crystallographica section A: crystal physics, diffraction, theoretical and general crystallography. 1976;32(5):751-67.
27. Qin. Fei, C. Chang D, Mao J. Alloy. Compd. 2005;390(1-2):134-137.
28. Frost RL, Bouzaid JM, Reddy BJ. Vibrational spectroscopy of the sorosilicate mineral hemimorphite $Zn_4(OH)_2Si_2O_7·H_2O$. Polyhedron. 2007;26(12):2405-12.
29. Chandrappa GT, Ghosh S, Patil KC. Synthesis and Properties of Willemite, Zn_2SiO_4, and M^{2+}:Zn_2SiO_4 (M= Co and Ni). Journal of Materials Synthesis and Processing. 1999;7(5):273-9.
30. Makreski G, Jovanovski B, Kaitner A, Gajovic T. Biljan, Vib. Spectrosc. 2007; 44:162.
31. Caracas R, Gonze X. Ab initio determination of the ground-state properties of $Ca_2MgSi_2O_7$ åkermanite. Physical Review B. 2003;68(18):184102.
32. Salim MA, Hussain R, Abdullah MS, Abdullah S, Alias NS, Ahmad Fuzi SA, Md Yusuf MN, Mahbor KM. Solid State Sci. Technol. 2009;17(2):59–64.
33. Erkul Karacaoglu, Bekir Karasu, Indian Journal of Chemistry. 2015;54A:1394-1401.
34. Lin L, Yin M, Shi C, Zhang W. Journal of Alloys and Compounds. 2008;455(1-2):327-330.
35. Zhu L, Zuo C, Luo Z, Lu A. Photoluminescence of Dy^{3+} and Sm^{3+}: SiO_2–Al_2O_3–LiF–CaF_2 glasses. Physica B: Condensed Matter. 2010;405(21):4401-6.
36. Chen Y, Cheng X, Liu M, Qi Z, Shi C. Comparison study of the luminescent properties of the white-light long afterglow phosphors: $Ca_xMgSi_2O_{5+x}$: Dy^{3+} (x= 1, 2, 3). Journal of luminescence. 2009;29(5): 531-5.
37. Sharma S, Dubey SK. The Significant Properties of Silicate Based Luminescent Nanomaterials in Various Fields of Applications: A Review. International Journal of Scientific Research in Physics and Applied Sciences. 2021;9(4):37-41.

Peer-review history:
The peer review history for this paper can be accessed here:
https://www.sdiarticle4.com/review-history/77207